PFG 2012 / 4, 0345–0358
Stuttgart, August 2012

Article

Accurate Reconstruction of Near-Epipolar Line Segments from Stereo Aerial Images

Ali Özgün Ok, Mersin, Turkey, Jan Dirk Wegner, Christian Heipke, Franz Rottensteiner, Uwe Sörgel, Hannover & Vedat Toprak, Ankara, Turkey

Keywords: line matching, line reconstruction, near epipolar line segments, projective geometry, stereo aerial images

Summary: In this study, a new 3D reconstruction approach for line segments from stereo images is proposed which covers the case that the image lines are nearly-aligned ($\leq 10^{o}$) with the epipolar line. The method manipulates the redundancy inherent in line pair-relations to generate artificial 3D points and utilizes those entities during the estimation process to improve the reconstruction of the line segments. The best points for the reconstruction are selected based on a newly proposed weight function. To test the performance of the proposed approach, we selected three test patches over a built-up area of the city of Vaihingen, Germany. The proposed approach produced a highly promising reconstruction performance for line segments that are nearly aligned with the epipolar line.

Zusammenfassung: In diesem Beitrag wird eine neue Methode zur 3D Rekonstruktion von Geraden aus Stereobildern vorgeschlagen, welche in den Bildern beinahe parallel ($\leq 10^{o}$) zur Kernlinie liegen. Die Redundanz, welche sich aus paarweisen Relationen von Linien ergibt, wird ausgenützt, um künstliche 3D Punkte zu erzeugen, die dann in die Schätzung der Parameter der 3D Linien als Beobachtungen eingehen und die Ergebnisse der Rekonstruktion verbessern. Die am besten für die Rekonstruktion geeigneten Punkte werden auf Basis einer neu entwickelten Gewichtsfunktion ausgewählt. Um die Leistungsfähigkeit des Verfahrens zu testen, wurden drei Testgebiete in einem bebauten Gebiet der Stadt Vaihingen (Baden-Württemberg) ausgewählt. Das Verfahren lieferte viel versprechende Ergebnisse für die Rekonstruktion von 3D Linien, die in den Bildern beinahe parallel zu den Epipolarlinien liegen.

1 Introduction

The matching and reconstruction of line segments in ultra-high resolution (3–10 cm) stereo aerial images is a very challenging task due to various reasons, e.g. substantial change in viewpoints, inconsistency of line endpoint locations, lack of rich textures in local line neighbourhood, repetitive patterns, etc. Up to now, a significant number of research papers have been devoted to stereo line matching, e.g. Schmid & Zisserman (1997), Baillard & Dissard (2000), Scholze et al. (2000), Zhang & Baltsavias (2000), Suveg & Vosselman (2004), Bay et al. (2005), Wang et al. (2009), Ok et al. (2010a, b). However, ultimately the problem has not been solved. In particular, in stereo geometry, the reconstruction of line segments that are nearly parallel to the epipolar lines is a challenging problem. The preferred way to alleviate this problem is to acquire more images, in particular with at least 60 % side lap. This type of overlapping image acquisition ensures the availability of at least one image in the cross-strip direction; thus, the problem of nearly collinear image perspective centers is mitigated, which comes along with better intersection angles of the projection planes. On the other hand, utilizing additional images in the cross-strip direction leads to new problems. Since those images are acquired in adjacent strips, there is a time delay between those images, which causes a difference in the illumination; thus, the moving

www.schweizerbart.de
DOI: 10.1127/1432-8364/2012/0122
1432-8364/12/0122 $ 3.50

shadow phenomenon occurs. As a result, the overall geometric quality of the final reconstruction is negatively affected (Haala 2009). Moreover, from an economical point of view, any increase of side-overlap during image acquisition results in longer flight times and increases costs. Therefore, from an operational perspective, the number of strips must be minimized and common side overlaps of about 30 % are still preferred and frequently used in many countries. For instance, the surveying authorities of the German Federal State of Lower Saxony still regularly acquire aerial images with a side lap of 30 % (LGLN 2012). For those reasons, accurate reconstruction of line segments from aerial images acquired in a stereo configuration has a major importance and in this paper, our focus is on this field of research.

Reconstructed 3D line segments can be used for applications such as the reconstruction of buildings (Scholze et al. 2002) and roads (Zhang 2004). Theoretically, object lines corresponding to slope changes or height discontinuities could also be detected in a dense DSM as it can be generated by modern dense matching techniques (Hirschmüller 2008). However, this is not the case for lines that are just defined by their radiometric differences from their surroundings; such lines are very useful for road extraction (Zhang 2004). Furthermore, dense matchers have problems with object planes that have no texture and that are not fronto-parallel, in particular if wide baselines are involved, because the smoothness term used in such methods will cause neighbouring pixels having similar grey values to have the same depth (Bulatov 2011). These problems and the fact that 3D lines provide a sparse representation of the information most relevant for the reconstruction of man-made objects motivate our interest in 3D line reconstruction.

The general strategy to solve line matching problems in stereo vision has relied on various descriptors specialized for one-to-one line matching. However, the integration of the line-to-line relations in the matching process does not only expose new constraints to improve the matching performance (Ok et al. 2010a, b), but also provides new opportunities for the reconstruction stage. In Ok et al. (2010a), we presented an approach for pair-wise matching of line segments from stereo aerial images, an approach that was extended to deal with repetitive linear patterns in Ok et al. (2010b). In this paper, we want to focus on the reconstruction of the matched segments. Although the method of direct construction (Heuel & Förstner 2001, Heuel 2001) gives satisfactory reconstruction results for lines that are not aligned with the epipolar line, a dramatic decrease in terms of accuracy for lines that are nearly or exactly aligned ($\leq 10^{o}$) with the epipolar line is inevitable (Fig. 1). This is due to the fact that if the angles of lines in image space get closer to the epipolar direction, the two projection planes generated from line segments become similar and in the worst case (exact alignment) become identical. For those cases, the direct construction of 3D lines from the intersection of planes may fail or at least produce inaccurate results. For that reason, Zhang (2005) proposed an alternative way which relies on free-form line structures. The major difficulty with the free-form structures is that the problematic line(s) must have an edge connection with the other neighbouring lines. However, this is rarely the case for most of the line segments. Therefore, in this paper, we propose a new reconstruction method that relies on the line-to-line relations developed in the pair-wise matching approach. The main idea is to manipulate the redundancy inherent in pair-relations to generate artificial 3D points from available pair matches and utilize those points during the estimation process to perform accurate reconstruction of the matched segments. However, since we do not know whether the two lines in a pair really intersect in object space or not, we select the point entities best suited for the estimation process by means of a new weight function which is composed of three main terms that are computed in a pair-wise manner: Euclidean distance, epipolar constraint and intersection angle in image space. For each problematic matching case ($\leq 10^{o}$), we automatically select the appropriate artificial 3D points and use the selected points in the estimation process along with the projection planes of the line segments. Thus, we can also reconstruct these problematic line segments with promising final accuracies.

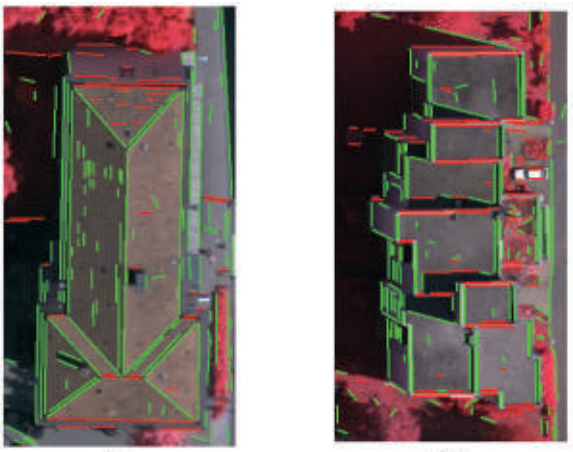

Fig. 1: The line segments extracted from two test patches. The red segments indicate the lines that are found to be nearly aligned (≤ 10°) with the epipolar line (flight direction).

The remainder of this paper is organized as follows. We shortly summarize the used stereo line matching approach in section 2. In section 3, the details of the proposed reconstruction approach are described. We present the test images and the results in section 4. Finally, in section 5 we give concluding remarks and make suggestions for future work.

2 Matching of Line Segments

For the matching of line features, we recently proposed a new relational approach in which the line correspondences between the aerial stereo images are established using pair-wise relations. In this paper, we only briefly summarize the matching algorithm and refer the reader to the references for further details (Ok et al. 2010a, b). The algorithm consists of three fundamental steps: (i) 2D line extraction, (ii) stereo matching of the extracted lines with a pair-wise relational approach, and (iii) iterative pair-based post-processing.

In the first step, the multispectral information existing in aerial images is fully utilized in order to maximize the performance of line detection. To accurately describe the straight edge segments, a principal component analysis technique was adapted and the parameters of the straight line segments are determined using orthogonal regression. In addition, during the raster-to-vector conversion, we allow curved structures to be approximated by piecewise linear representations. In the second step, a new pair-wise stereo line matching approach is used to establish the pair-wise line correspondences between the stereo images. The approach initially generates reference line pairs in the base image and collects all potential matching candidate pairs from the search image with the aid of a-priori known image-to-image geometry. Next, the number of matching candidate pairs of each line pair in the base image is significantly reduced after imposing a weighted pair-wise matching similarity score computed over a total of eight pair-wise constraints (an epipolar, three geometric, two photometric, a correlation and a spatiogram constraint). In the last step, an iterative pair-based post-processing algorithm is utilized. For each line in the base image, the best corresponding line in the search image is found in an iterative disambiguation process in which the matching inconsistencies are further eliminated using nearest/next distance ratios and a final similarity voting scheme (Ok et al. 2010a, b).

3 Reconstruction of Line Segments

The reconstruction process starts with a test which determines the angle difference (0°–90°) between the line segments and the related epipolar line. Based on our experiences, the line segments that have angle differences of less than 10° are highly susceptible to produce inaccurate reconstruction results. Fig. 2 clarifies this fact. In the figure, the RMS distances of direct reconstruction results from lidar data are plotted as a function of the angle differences for all line segments correctly matched in test patch 1 used in our experiments (see the details of the comparison method in section 4). As can be seen from Fig. 2a, the best reconstruction performance is achieved for the line segments that have angle differences of 60° or more (≈ 1 pixel). However, the line segments that have angle differences of 10° or less provided extremely large overall RMS distances. Therefore, during the test, we label the line segments as not-aligned if the angle difference is larger than 10°. The reconstruction of all those matched line segments is performed by intersecting the projection planes (Fig. 3a), $\mathbf{A}^1(l_1)$ and $\mathbf{A}^2(l_2)$. The intersection is carried out with the method of direct construction (Heuel & Förstner 2001, Heuel 2001), which is an algebraic approach used for the construction of the 3D lines directly from given plane entities.

The underlying approach for the reconstruction of line segments that are nearly-aligned (≤ 10°) with the epipolar line is to manipulate the redundancy inherent in pair-relations (Ok et al. 2010b) to generate artificial 3D points ($\mathbf{X}_i$) and utilize those points in the estimation process. In this way, the neighbouring line segments that have line pair-connections with the problematic segment contribute to the reconstruction (Fig. 3b). As we shall see in the subsequent section, all generated points lie exactly on the problematic line segments in image space and, thus, also belong to the projection planes. Therefore, each artificial 3D point $\mathbf{X}_i$ must be generated beforehand, and the final estimation will consider these points jointly with the projection planes ($\mathbf{A}_i$). In this section, we follow the representation of the homogeneous uncertain vectors given in (Heuel & Förstner 2001).

3.1 *The Generation of Uncertain Artificial 3D Point Entities*

Formally the uncertain homogeneous vectors are denoted as $(\mathbf{x}, \boldsymbol{\Sigma}_{xx})$, where $\boldsymbol{\Sigma}_{xx}$ is the covariance matrix of the homogeneous vector $\mathbf{x} = [u_x, v_x, w_x]^T$. A 2D uncertain line $(\mathbf{l}, \boldsymbol{\Sigma}_{ll})$ in image space can be generated by joining the endpoints of the line segment, $(\mathbf{x}, \boldsymbol{\Sigma}_{xx})$ and $(\mathbf{y}, \boldsymbol{\Sigma}_{yy})$:

$$\left(\mathbf{l}, \boldsymbol{\Sigma}_{ll}\right) = \left(\mathbf{x} \times \mathbf{y},\ \mathrm{S}(\mathbf{y})\boldsymbol{\Sigma}_{xx}\mathrm{S}(\mathbf{y})^T + \mathrm{S}(\mathbf{x})\boldsymbol{\Sigma}_{yy}\mathrm{S}(\mathbf{x})^T\right)$$

$$\mathrm{S}(\mathbf{x}) = \begin{bmatrix} 0 & -w_x & v_x \\ w_x & 0 & -u_x \\ -v_x & u_x & 0 \end{bmatrix} \quad (1)$$

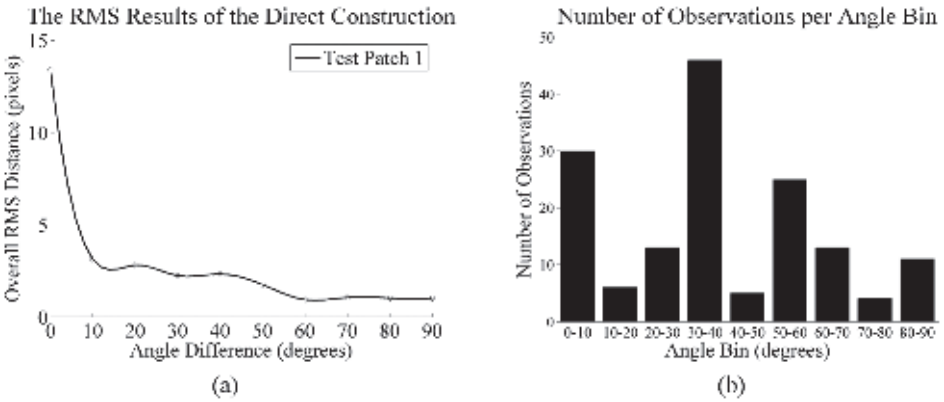

Fig. 2: (a) The performance of the direct construction method for various angle differences (0°–90°), and (b) the number of observations of line versus plane comparison used to generate RMS results in Fig. 2a.

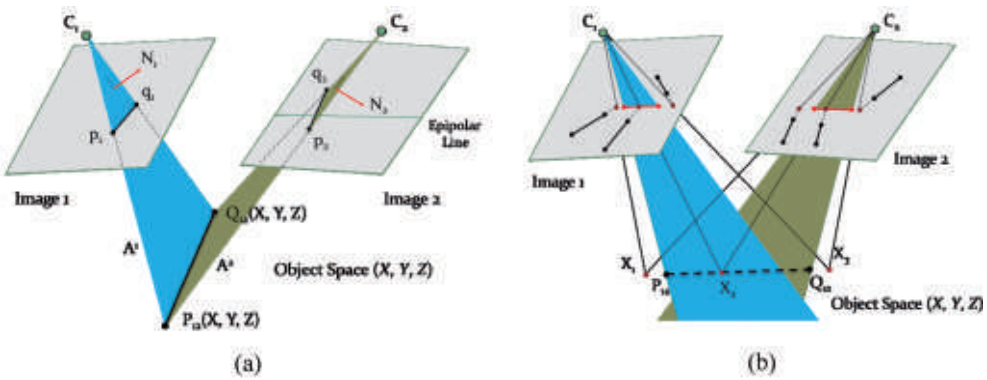

Fig. 3: The reconstruction of the line segments (a) that are not aligned with the epipolar line, and (b) that are nearly-aligned with the epipolar line. In (b), a dashed line style is used to illustrate that the line segment in object space is between the two projection planes.

where the skew-symmetric matrices S(**x**) and S(**y**) are the matrix representations of the vector cross product with the points **x** and **y**, respectively. Similar to (1), the intersection point **x** of two lines **l** and **m** can be computed as

$$\left(\mathbf{x}, \boldsymbol{\Sigma}_{xx}\right) = \left(\mathbf{l} \times \mathbf{m},\ \mathrm{S}(\mathbf{l})\boldsymbol{\Sigma}_{mm}\mathrm{S}(\mathbf{l})^{\mathrm{T}} + \mathrm{S}(\mathbf{m})\boldsymbol{\Sigma}_{ll}\mathrm{S}(\mathbf{m})^{\mathrm{T}}\right) \quad (2)$$

with the related skew-symmetric matrices, S(**l**) and S(**m**). In our case, initially, the covariance matrices of line endpoints are computed from edges that form the line segment in the way described in (Madsen & Christensen 1995). Next, the lines and their uncertainties are computed from those endpoints using (1) (Fig. 4a). Thereafter, for each problematic segment, the neighbouring line segments that have a pair-connection with the problematic segment are collected from the available pairwise matches, and their intersection points are computed using (2). Fig. 4b illustrates an example of a generated artificial intersection point with its elliptical confidence region.

The estimation of the artificial 3D points $\mathbf{X}_i$ from 2D correspondences cannot be performed using direct construction, because the

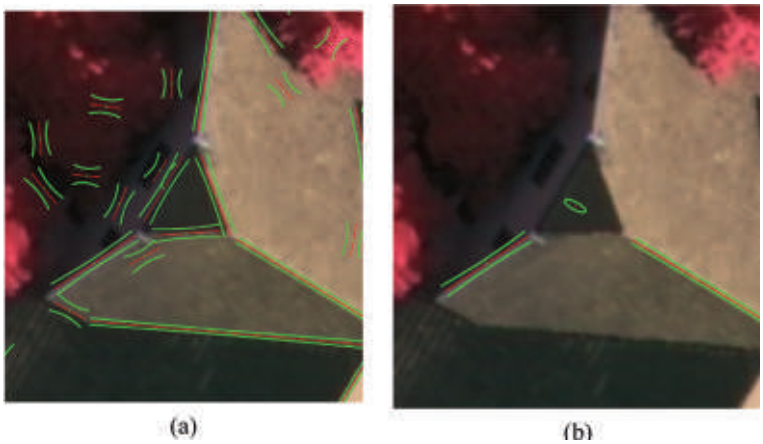

Fig. 4: (a) Confidence regions of extracted line segments, (b) an example of the generated artificial intersection point and its elliptical confidence region. Entities and confidence regions are shown in red and green colours, respectively. Confidence regions are 15 times exaggerated for visualization.

projecting rays emerging from 2D points rarely intersect in object space. Therefore, we estimate the 3D points using the iterative linear Gauss-Helmert model with constraints (McGlone et al. 2004, Förstner 2005). We have six observations per point (two homogeneous 3D vectors $\mathbf{x}_{ij}$ per image point, where j is the image index) and four unknowns, i.e. the homogeneous coordinates of the 3D point. Thus, referring to the Gauss-Helmert model, we have the vector γ of the observations and the vector β of the unknown parameters:

$$\boldsymbol{\gamma}_{6\times1}=\begin{bmatrix}\mathbf{x}_{i1}\\ \mathbf{x}_{i2}\end{bmatrix} \qquad \boldsymbol{\beta}_{4\times1}=\mathbf{X}_i \tag{3}$$

The information that a point $\mathbf{X}_i$ has to be on the image ray emanating from point $\mathbf{x}_{ij}$ in image j can be used to formulate three constraint equations $S(\mathbf{x}_{ij})\, P_j\, \mathbf{X}_i = 0$, where P_j is 3x4 projection matrix for points on image j. Of these three equations, only two are independent. In this study, we describe the independent constraints of $S(\mathbf{x})_{3x3}$ with reduced skew-symmetric matrices $S^r(\mathbf{x})_{2x3}$. Two independent constraints can be selected by choosing those two which belong to the rows of $S(\mathbf{x})$ containing the absolute largest element of the vector $\mathbf{x}$, at the same time being the largest element in $S(\mathbf{x})$ (McGlone et al. 2004). Thus, there are two independent constraints $\boldsymbol{g}$ for each observed image point $\mathbf{x}_{ij}$ and the unknown parameters ($\mathbf{X}_i$). In addition, we have a single length constraint h on the unknown parameters due to the homogeneity of $\mathbf{X}_i$. Thus, the relations of the Gauss-Helmert model for the estimation of the 3D point entities can be written as:

$$\boldsymbol{g}(\boldsymbol{\beta},\boldsymbol{\gamma})_{4\times1}=\begin{bmatrix}S^r(\mathbf{x}_{i1})P_1\mathbf{X}_i\\ S^r(\mathbf{x}_{i2})P_2\mathbf{X}_i\end{bmatrix}=0 \tag{4}$$

$$h(\boldsymbol{\beta})=\mathbf{X}_i^{\mathrm{T}}\mathbf{X}_i-1=0$$

The initial approximate values of $\mathbf{X}_i$ for the iterative solution can be obtained from the singular value decomposition (SVD) solution (Heuel & Förstner 2001) which is a common method used to solve a set of homogeneous linear equations. Once the estimation is completed, the covariance matrices of the estimated 3D point entities can be computed from the inverted normal equation matrix.

3.2 *The Joint Estimation of the 3D Line Segments*

For the estimation procedure, we parameterize the 3D lines in Plücker representation $\boldsymbol{L}^T = (\boldsymbol{L}_h^T, \boldsymbol{L}_0^T) = (L_1, L_2, L_3, L_4, L_5, L_6)$ (McGlone et al. 2004) and utilize an iterative linear Gauss-Markoff model with constraints. The algebraic expressions of the form $\mathbf{g}_i(\beta; \gamma_i) = 0$ with respect to all possible observation (γ_i) and unknown (β) entities are developed and explicitly given in Förstner et al. (2000) and Heuel & Förstner (2001). In our case, we are searching for an unknown line $\mathbf{M}$ which primarily must lie in two planes; thus,

$$\mathbf{g}_1\left(\mathbf{M};\mathbf{A}_i\right)_{4x1}=\Pi^{\mathrm{T}}\left(\mathbf{A}_i\right)\mathbf{M}=0 \tag{5}$$

where i is the plane index and Π^{T} is the homogeneous matrix representation:

$$\Pi^{\mathrm{T}}\left(\mathbf{A}_i\right)=\begin{bmatrix}A_{i0}\mathbf{I}_n & S^{\mathrm{T}}(\mathbf{A}_{ih})\\ -\mathbf{A}_{ih}^{\mathrm{T}} & \mathbf{0}^{\mathrm{T}}\end{bmatrix} \tag{6}$$

In (6), $\mathbf{A}_{ih}$ and $\mathbf{A}_{i0}$ correspond to homogeneous and Euclidean components of the plane $\mathbf{A}_i$, and $\mathbf{I}_n$ is a 3 x 3 identity matrix. The projection planes $\mathbf{A}_i$ for each line $\mathbf{l}_i$ and the related uncertainties can be determined using the projection matrices P_j of the images:

$$\mathbf{A}_i=P_j^{\mathrm{T}}\mathbf{l}_i$$

$$\Sigma_{A_iA_i}=P_j\Sigma_{l_il_i}P_j^T+\left(I_4\otimes\mathbf{l}_i\right)\Sigma_{P_jP_j}\left(I_4\otimes\mathbf{l}_i^{\mathrm{T}}\right) \tag{7}$$

where $\mathbf{I}_n$ represents n x n unit matrix and $\otimes$ denotes the Kronecker product. The uncertainty of each line is derived from (1) and for this study; we assume that the projection matrices are free of error. In addition to the projection planes, the unknown line should also contain the artificial 3D points $\mathbf{X}_i$ generated from the neighbouring line segments:

$$\mathbf{g}_2\left(\mathbf{M};\mathbf{X}_i\right)=\overline{\Pi}^{\mathrm{T}}\left(\mathbf{X}_i\right)\mathbf{M}=0 \tag{8}$$

where i is the point index and $\overline{\Pi}^{\mathrm{T}}$ is the homogeneous matrix representation:

$$\overline{\Pi}^{\mathrm{T}}\left(\mathbf{X}_i\right)=\begin{bmatrix}-S(\mathbf{X}_{i0}) & X_{ih}\mathbf{I}_n\\ -\mathbf{X}_{i0}^{\mathrm{T}} & \mathbf{0}^{\mathrm{T}}\end{bmatrix} \tag{9}$$

In (9), X_{ih} and $\mathbf{X}_{i0}$ correspond to homogeneous and Euclidean components of the points $\mathbf{X}_i$ and $\mathbf{I}_n$ is a 3 x 3 identity matrix. However, since we do not exactly know whether the two lines in a pair really intersect in object space or not, before the estimation process we compute a weight for each artificial 3D point. The weights depend on three measures computed in a pair-wise manner, namely the minimum 2D Euclidean distance (d_{ij}) between two line segments (l_i and l_j, where i and j represents the line indices), the minimum angle (θ_{ij}) enclosed by line segments l_i and l_j, and the minimum orthogonal distance (d^e_{ij}) between the intersection points and related epipolar lines (l_{epi}) (Fig. 5a). The minimum 2D Euclidean distance (d_{ij}) between the two line segments is computed in a distinctive way in which the edge segments that form the line segments are taken into account (Fig. 5b). To do that, first, edge segments are labelled by 8-neighbourhood pixel connectivity, and after that, all edge-to-edge distances between line segments are evaluated. Finally, the distance which provides the minimum distance between the two edge segments is selected as the minimum 2D Euclidean distance. For example, in Fig. 5b, the distance between the line segments l_1 and l_2 is computed as zero since they belong to the same edge segment. In this way, we fully take into account the information of edge connectivity (or edge proximity) for the line segments during the computation of the minimum 2D distances in image space.

In principle, the reliability of a point increases if the distances (both d_{ij} and d^e_{ij}) computed are relatively short and decreases if the intersection angle is quite narrow (e.g., < 10º). Therefore, we designed the new cumulative weight function (W_i) as:

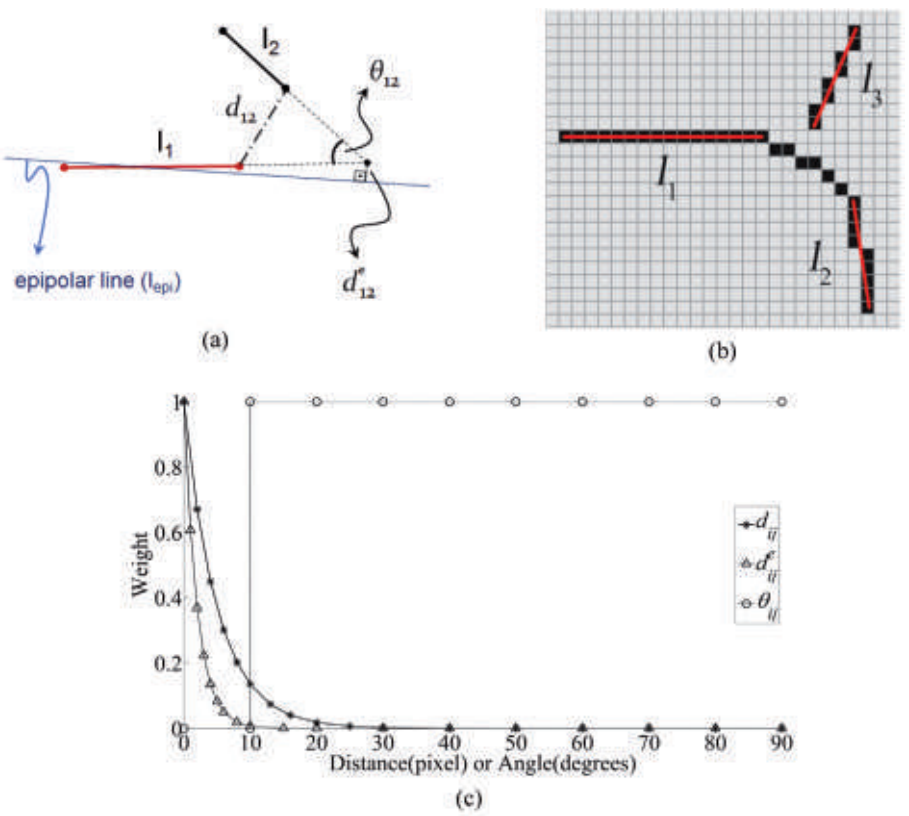

Fig. 5: (a) Three measures used in the weight function, (b) the computation of minimum 2D distances in image space, and (c) independent weight curves for each measure. The control parameters are utilized as $\sigma_1 = 5$ and $\sigma_2 = 2$.

$$W_i = t_{ij}.e^{-\left(\frac{\sigma_2 d_{ij}+\sigma_1 d_{ij}^e}{2\sigma_1\sigma_2}\right)}$$

$$t_{ij} = \begin{cases} 0 & \text{if } \theta_{ij} \le 10° \\ 1 & \text{if } \theta_{ij} > 10° \end{cases} \quad (10)$$

where the parameters σ_1 and σ_2 control the weighting for the metrics d_{ij} and d_{ij}^e, respectively. Empirically, we found that the points which have distances of d_{ij} > 30 pixels or d_{ij}^e > 10 pixels are not reliable for the estimation process. Therefore, the control parameters σ_1 and σ_2 in (10) are selected as 5 and 2, respectively. Fig. 5c shows the weighting curves computed separately for each measure. As can be seen in Fig. 5c, the exponential function used for the distance d_{ij}^e rapidly decreases with an increase of the computed 2D Euclidean distances and reduces to a weight value of almost zero at a d_{ij}^e distance value of 10 pixels. Besides, the exponential weight function used for the distance d_{ij} reduces to almost zero weight value when the distance d_{ij} is 30 pixels. On the other hand, for the angle parameter θ_{ij}, a piecewise constant function with a single interval at 10º guarantees that the artificial 3D points generated from two neighbouring line segments are computed with intersection angles of larger than 10º.

For each nearly-aligned matching case (≤ 10º), the artificial 3D points $\mathbf{X}_i$ are collected and their weights W_i are determined using (10). However, it is not logical to integrate all observed point entities directly to the estimation process, since some of those points may be generated from wrong matches. Therefore, first, we eliminate all point entities that have weights less than a pre-defined threshold ($T_w \le 0.05$). Thereafter, among the remaining points, only the points that have the highest weights are integrated to the estimation process along with the observed projection planes. However, the selection approach for the best point entities is not trivial, since the spatial distribution of the 3D points eventual-

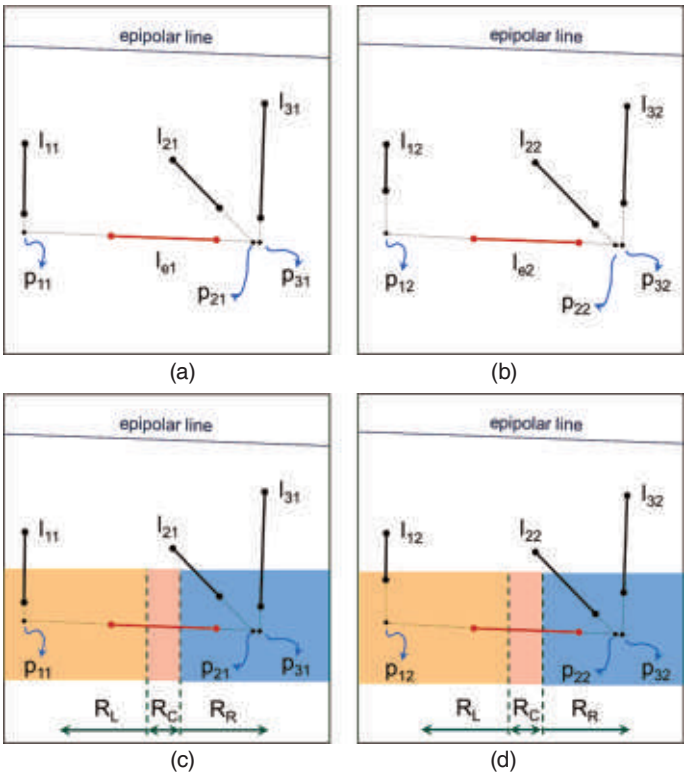

Fig. 6: Left (a, c) and right (b, d) stereo images. The directional regions utilized during the selection of the best weighted point entities.

ly determines the quality of the estimated 3D line. Fig. 6 clarifies this fact. In the figure, the line segments l_{e1} and l_{e2} are nearly aligned to the epipolar lines. After pair-wise matching, assume that l_{e1} and l_{e2} are correctly matched and have pair-relations with three neighbouring line segments (l_1, l_2, and l_3). We estimate the related 3D points ($\mathbf{X}_1$, $\mathbf{X}_2$, and $\mathbf{X}_3$) from the corresponding intersection points (p_{ij}) using (1)–(4) and compute the related weights (W_1, W_2 and W_3) for each point from (10). It is clear that the points $\mathbf{X}_2$ and $\mathbf{X}_3$ will get higher weights than $\mathbf{X}_1$, because, assuming no edge connectivity, the computed minimum 2D Euclidean distance (d_{ij}) measure for $\mathbf{X}_1$ is significantly larger than the other distances. Thus, in this case, the 3D line would be estimated from $\mathbf{X}_2$ and $\mathbf{X}_3$ along with the projection planes $\mathbf{A}_{e1}$ and $\mathbf{A}_{e2}$. However, since those entities are very close to each other and are located just on one side (to the right) of the lines l_{e1} and l_{e2}, the final position of the line segments in object space is highly sensitive to the small deviations between the entities $\mathbf{X}_2$ and $\mathbf{X}_3$, which may significantly reduce the final accuracy of the estimated 3D line. To solve this problem, we propose a region-based weighting of points (Fig. 6 c, d). We utilize two split points ($l/3$, $2l/3$) to divide the line into three directional regions, left (R_L) – centre (R_C) – right (R_R). Next, for each region independently, the point having the highest weight is searched and utilized in the estimation process. Thus, we guarantee that the point $\mathbf{X}_i$ generated by the intersection points p_{l1} and p_{l2} contributes to the final estimation.

For the estimation process, we form the point-line and plane-line incidence relations in 3D space and perform an iterative linear Gauss-Markoff model with constraints. For each case, we have 6 unknowns (Plücker coordinates) and 2 constraints (Plücker constraint and length) for each 3D line ($\mathbf{L}_i$). In addition to the two projection planes, the final observation number depends on the number of point entities $\mathbf{X}_i$ available for each region. Once again, the required initial values can be taken from the SVD solution, and the covariance matrices of the estimated 3D line entities can be computed from the inverted normal equation matrix of the Gauss-Markoff model.

4 Test Sites and Results

Three test patches (Fig. 7) are chosen from the DGPF test site in Vaihingen, Germany (Cramer 2010). For those test patches, stereo images were acquired by the DMC digital camera with 800 m flying height, which corresponds to a ground sample distance (GSD) of approximately 8 cm. The images were acquired with 70 % forward overlaps with a base-to-height (B/H) ratio of 0.28.

During the experiments, for all test patches, we applied a 50 m (≈ 162 pixels) search range difference (between the min. and max. heights) along the epipolar lines. In order to assess the performance of the line matching, the line matches were classified into three categories: True Positive (TP), False Positive (FP), and False Negative (FN), by comparing the automatically matched line segments with the manually generated reference line matching list. We term a line match as a True Positive if that match correctly corresponds to a matching relation in the reference list. On the other hand, a False Positive is a line match that does not correspond to any of the line matches in the reference list, and a False Negative is a line match that exists in the reference list but cannot be found by the automated approach.

Tab. 1: The matching performance of the pair-wise approach (TP = true positive, FP = false positive, FN = false negative).

Patch ID	Number of			Level of		
	TP	FP	FN	Correctness	Completeness	Quality
1	101	3	2	97 %	98 %	95 %
2	94	6	5	94 %	95 %	90 %
3	111	5	14	96 %	89 %	85 %

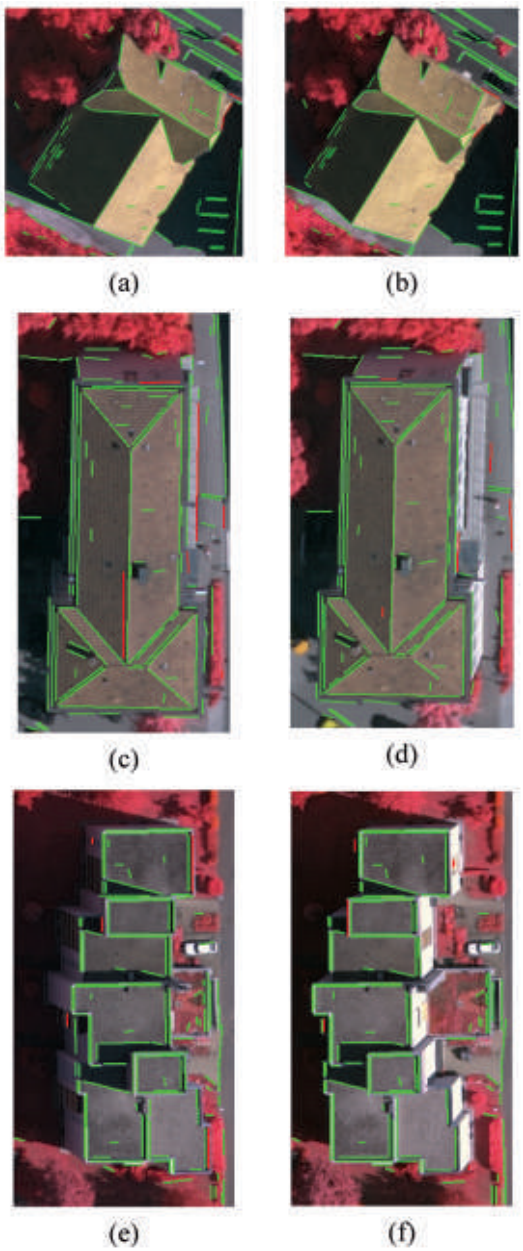

Fig. 7: Test patches. Left (a, c, e) and right (b, d, f) stereo images. Correct and false matches are shown in green and red colours, respectively.

In this study, we follow the well-known three metrics (correctness, completeness, and quality) (Rutzinger et al. 2009) to evaluate the quality of the line matching (Tab. 1). In all test patches, consistent correctness levels (> 94 %) are achieved. Similarly, the computed completeness levels for all patches are comparable. The highest number of FNs is found in the third test patch. This is due to the nature of the pair-wise approach: most of those FNs are located on the ground level and could not be paired correctly with other ground level line segments because of many obscured regions.

Despite the successful matching, the method of direct construction produced dramatic reconstruction problems for the lines that are nearly-aligned with the epipolar line (Fig. 8 a, d, g). It is clear from those figures that the reconstruction results of the line segments that are nearly-aligned with the epipolar line are extremely defective and irrelevant. On the other hand, our approach successfully recovered most of those problematic cases (Fig. 8 b, e, h). Although we believe that the level of improvement is visually apparent, we also evaluated the accuracy of the reconstructed line segments by comparing them to lidar data. The lidar data of the test site were captured with a Leica ALS50 system with an accuracy of 3–4 cm (Haala et al. 2010). In order to compare the reconstructed lines, we automatically extracted 3D planes from the point cloud in the vicinity of each line (Fig. 8 c, f, i). Depending on the type of the line, this plane reconstruction process resulted in one plane if the line corresponded to a step edge and in two planes if the line corresponded to the intersection of two planes. Thereafter, we determined the line's average orthogonal distance from its neighbouring planes and used these distances to compute the RMS average distance between the reconstructed lines and the lidar planes. The results for each patch are given in Tab. 2. As expected, the method of direct construction produced reasonable RMS distances (≈ 2 GSD) for the line segments that are not aligned with the epipolar line. On the other hand, large RMS distances (> 1 m) are inevitable for the nearly-aligned cases, which also reduce the overall performance considerably. In contrast to the results of the direct construction, for each test patch, our approach led to a considerable improvement of the RMS values after the reconstruction of the nearly-aligned line segments. Not surprisingly, in each case, this achievement also improves the overall RMS performance which is in the order of 2–3 GSD.

5 Conclusions

In this paper, we proposed a new reconstruction method for the line segments whose orientations in image space are found to be similar to the orientation of the epipolar line. The method manipulates the redundancy inherent in line-pair relations to generate artificial 3D points and utilize those entities in the estimation process to improve the accuracy of the reconstructed line segments. To test our approach, we selected three test patches over a built-up area of the city of Vaihingen, Germany. Based on the results, the proposed approach produced highly promising reconstruction results for the line segments that

Tab. 2: Comparison of the computed RMS distances of the Direct Construction method and the Proposed Approach. The numbers in brackets show the total number of planes used to compute the RMS distances.

Patch ID	Number of Planes Found		RMS Average Distance (m)					
			Direct Construction			Proposed Approach		
	Not Aligned	Nearly Aligned	Not Aligned	Nearly Aligned	Total	Not Aligned	Nearly Aligned	Total
1	153	30	0.152	1.041	0.495	0.152	0.357	0.204
2	85	27	0.173	4.451	2.240	0.173	0.196	0.179
3	119	32	0.194	6.278	3.768	0.194	0.459	0.275

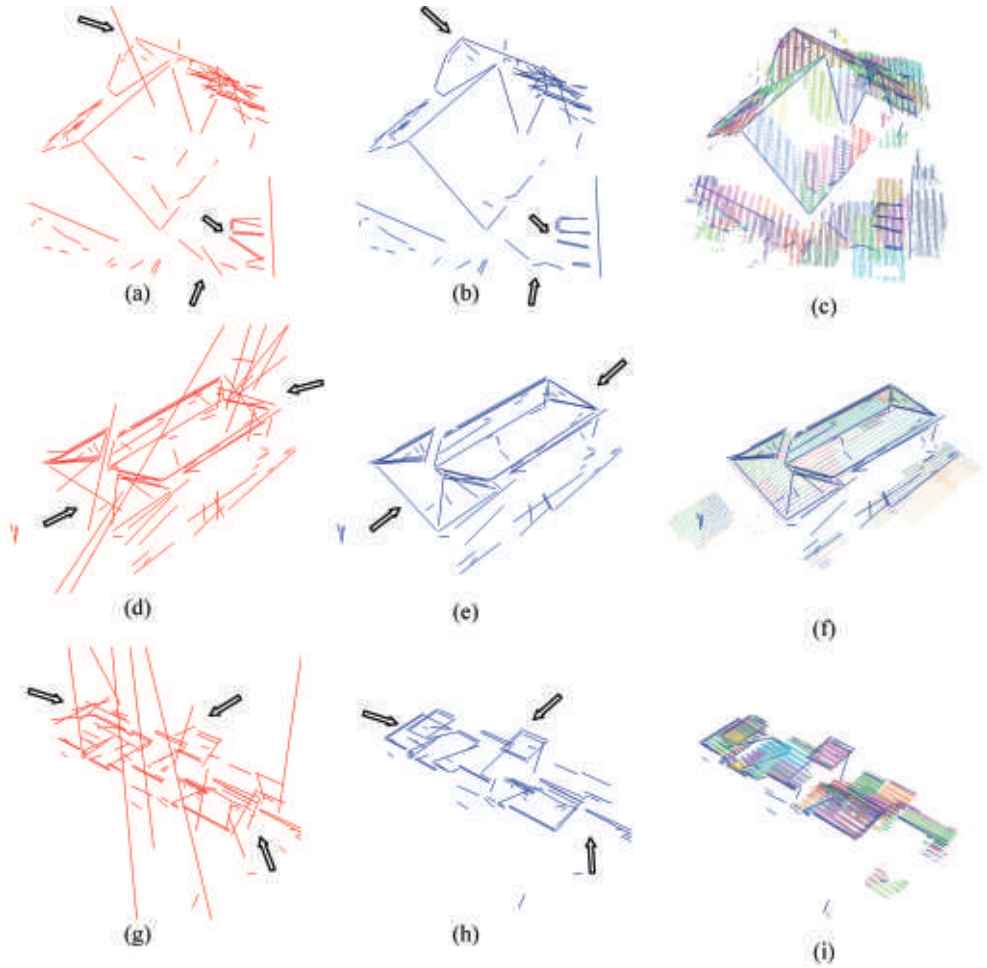

Fig. 8: 3D line segments generated with the method of direct construction (a, d, g) and our approach (b, e, h). Block arrows point to parts where some of the critical improvements are observed. The lidar point cloud overlaid with the lines reconstructed with our approach (c, f, i). Each colour in the point cloud belongs to the automatically extracted 3D planes in the vicinity of each line.

are nearly-aligned with the epipolar line. Indeed, the final improvement is considerable in terms of RMS distances, considering that the results of the previous approaches that just rely on direct construction consistently result in large RMS distances (> 1 m). Compared to the direct construction method, the gross errors are particularly reduced by the proposed approach, and an overall RMS performance of about 2–3 GSD is achieved. It is obvious that the selected 3D points $\mathbf{X}_i$ improve the final quality of the 3D line during the estimation process. In a worst-case scenario in which only a single 3D point entity is available, our method will not perform worse than the standard direct construction.

As a future work, it is a fact that the reconstruction of straight line segments which are nearly parallel to the epipolar line is also numerically unstable within a single image strip. Therefore, currently, we are extending the approach to deal with reconstruction drawbacks observed in image triplets that are acquired within a single strip, and the extended approach is expected to provide further improvements for the reconstruction of the near-epipolar line segments in aerial image triplets.

Acknowledgements

The Vaihingen dataset was provided by the German Society for Photogrammetry, Remote Sensing and Geoinformation (DGPF) (Cramer 2010): http://www.ifp.uni-stuttgart.de/dgpf/dkep-allg.html.

References

Baillard, C. & Dissard, O., 2000: A Stereo Matching Algorithm for Urban Digital Elevation Models. – Photogrammetric Engineering and Remote Sensing **66** (9): 1119–1128.

Bay, H., Ferrari, V. & Van Gool, L., 2005: Wide-baseline Stereo Matching with Line Segments. – IEEE Computer Society Conference on Computer Vision and Pattern Recognition **1:** 329–336.

Bulatov, D., 2011: Textured 3D Reconstruction of Urban Terrain from UAV-borne Video Sequences. – PhD thesis, Wissenschaftliche Arbeiten der Fachrichtung Geodäsie und Geoinformatik der Leibniz Universität Hannover, Germany, **291**.

Cramer, M., 2010: The DGPF Test on Digital Aerial Camera Evaluation – Overview and Test Design. – PFG **2010** (2): 73–82.

Förstner, W., Brunn, A. & Heuel, S., 2000: Statistically Testing Uncertain Geometric Relations. – Sommer, G., Krüger, N. & Perwass, C. (eds.): Mustererkennung DAGM: 17–26, Springer.

Förstner, W., 2005: Uncertainty and Projective Geometry. – Bayro Corrochano, E. (ed.): Handbook of Geometric Computing: 493–535.

Haala, N., 2009: Come Back of Digital Image Matching. – Photogrammetric Week **2009:** 289–301, Wichmann Verlag, Heidelberg.

Haala, N., Hastedt, H., Wolf, K., Ressl, C. & Baltrusch, S., 2010: Digital Photogrammetric Camera Evaluation – Generation of Digital Elevation Models. – PFG **2010** (2): 99–116.

Heuel, S. & Förstner, W., 2001: Matching, Reconstructing and Grouping 3d Lines from Multiple Views Using Uncertain Projective Geometry. – IEEE Computer Vision and Pattern Recognition **2:** 517–524.

Heuel, S., 2001: Points, Lines and Planes and their Optimal Estimation. – Radig, B. & Florczyk, S. (eds.): DAGM, LNCS **2191:** 92–99, Springer, München.

Hirschmüller, H., 2008: Stereo Processing by Semi-global Matching and Mutual Information. – IEEE Transactions on Pattern Analysis and Machine Intelligence **30** (2): 328–341.

LGLN, 2012: Landesamt für Geoinformation und Landentwicklung Niedersachsen (LGLN), Digitale und Orientierte Luftbilder. http://www.lgn.niedersachsen.de/portal/live.php?navigation_id=11077&article_id=51723&_psmand=35 (30.1.2012).

Madsen, C.B. & Christensen, H.I., 1995: Modeling and Testing the Stability of Edge Segments: Length and Orientation. – Scandinavian Conference on Image Analysis: 1011–1019.

McGlone, C., Mikhail, E. & Bethel, J., 2004: Manual of Photogrammetry. – 5th ed., published by the American Society for Photogrammetry and Remote Sensing.

Ok, A.Ö., Wegner, J.D., Heipke, C., Rottensteiner, F., Sörgel, U. & Toprak, V., 2010a: A New Straight Line Reconstruction Methodology From Multi-Spectral Stereo Aerial Images. – The International Archives of the Photogrammetry, Remote Sensing and Spatial Information Sciences **38** (3A): 25–30.

Ok, A.Ö., Wegner, J.D., Heipke, C., Rottensteiner, F., Sörgel, U. & Toprak, V., 2010b: A Stereo Line Matching Technique For Aerial Images Based on A Pair-Wise Relation Approach. – The International Archives of the Photogrammetry, Remote Sensing and Spatial Information Sciences **38** (1/W17), Istanbul (on CD-ROM).

Rutzinger, M., Rottensteiner, F. & Pfeifer, N., 2009: A Comparison of Evaluation Techniques for Building Extraction from Airborne Laser Scanning. – IEEE Journal of Selected Topics in Applied Earth Observations and Remote Sensing **2** (1): 11–20.

Schmid, C. & Zisserman, A., 1997: Automatic Line Matching Across Views. – Computer Vision and Pattern Recognition: 666–671.

Scholze, S., Moons, T., Ade, F. & Van Gool, L., 2000: Exploiting Colour for Edge Extraction and Line Segment Stereo Matching. – The International Archives of the Photogrammetry, Remote Sensing and Spatial Information Sciences: 815–822.

Scholze, S., Moons, T. & Van Gool, L., 2002: A Generic 3D model for Automated Building Roof Reconstruction. – The International Archives of Photogrammetry and Remote Sensing **34** (5): 204–209.

Suveg, I. & Vosselman, G., 2004: Reconstruction of 3D Building Models from Aerial Images and Maps. – ISPRS Journal of Photogrammetry and Remote Sensing **58** (3-4): 202–224.

Wang, Z., Wu, F. & Hu, Z., 2009: MSLD: A Robust Descriptor for Line Matching. – Pattern Recognition **42** (5): 941–953.

Zhang, C. & Baltsavias, E.P., 2000: Edge Matching and 3D Road Reconstruction Using Knowl-